CANCER

DNA damage induces p53-independent apoptosis through ribosome stalling

Nicolaas J. Boon[1,2], Rafaela A. Oliveira[1,2]†, Pierré-René Körner[1,3]†, Adva Kochavi[1,3]†,
Sander Mertens[1,4], Yuval Malka[1,3], Rhianne Voogd[5], Suzanne E. M. van der Horst[1,4],
Maarten A. Huismans[1,4], Lidwien P. Smabers[6], Jonne M. Draper[2], Lodewyk F. A. Wessels[1,7],
Peter Haahr[1,2,8], Jeanine M. L. Roodhart[6], Ton N. M. Schumacher[1,5], Hugo J. Snippert[1,4],
Reuven Agami[1,3]*, Thijn R. Brummelkamp[1,2]*

In response to excessive DNA damage, human cells can activate p53 to induce apoptosis. Cells lacking p53 can still undergo apoptosis upon DNA damage, yet the responsible pathways are unknown. We observed that p53-independent apoptosis in response to DNA damage coincided with translation inhibition, which was characterized by ribosome stalling on rare leucine-encoding UUA codons and globally curtailed translation initiation. A genetic screen identified the transfer RNAse SLFN11 and the kinase GCN2 as factors required for UUA stalling and global translation inhibition, respectively. Stalled ribosomes activated a ribotoxic stress signal conveyed by the ribosome sensor ZAKα to the apoptosis machinery. These results provide an explanation for the frequent inactivation of SLFN11 in chemotherapy-unresponsive tumors and highlight ribosome stalling as a signaling event affecting cell fate in response to DNA damage.

Tumour protein P53 (*TP53*) is the most frequently mutated gene in human cancer and is referred to as the "guardian of the genome" (*1*, *2*). The p53 protein can be activated by DNA damage and functions as a transcription factor to induce a cell cycle arrest, allowing damage repair, or to induce apoptosis (*3*). Cancer treatments that eliminate tumor cells by damaging their DNA, such as radiotherapy or chemotherapeutics, can activate the p53 protein (*1*–*3*). However, the presence of wild-type *TP53* does not predict sensitivity to chemotherapeutics in large cell line panels (*4*) and cells with a defective p53 pathway can undergo apoptosis in response to DNA damage, although a clear understanding of the involved pathways is unavailable (*5*, *6*). Understanding these pathways could be relevant because 30 to 50% of all cancers contain mutant *TP53* (*7*), and such tumors are still treated using genotoxic therapies irrespective of these mutations. Thus, we explored the p53-independent mechanism(s) that activates apoptosis in response to DNA-damaging treatments.

[1]Oncode Institute, Utrecht, Netherlands. [2]Division of Biochemistry, Netherlands Cancer Institute, Amsterdam, Netherlands. [3]Division of Oncogenomics, Netherlands Cancer Institute, Amsterdam, Netherlands. [4]Center for Molecular Medicine, University Medical Center Utrecht, Utrecht, Netherlands. [5]Department of Molecular Oncology and Immunology, Netherlands Cancer Institute, Amsterdam, Netherlands. [6]Department of Medical Oncology, University Medical Center Utrecht, Utrecht University, Utrecht, Netherlands. [7]Division of Molecular Carcinogenesis, Netherlands Cancer Institute, Amsterdam, Netherlands. [8]Center for Gene Expression, Department of Cellular and Molecular Medicine, Faculty of Health and Medical Sciences, University of Copenhagen, Copenhagen, Denmark.
*Corresponding author. Email: r.agami@nki.nl (R.A.); t.brummelkamp@nki.nl (T.R.B.)
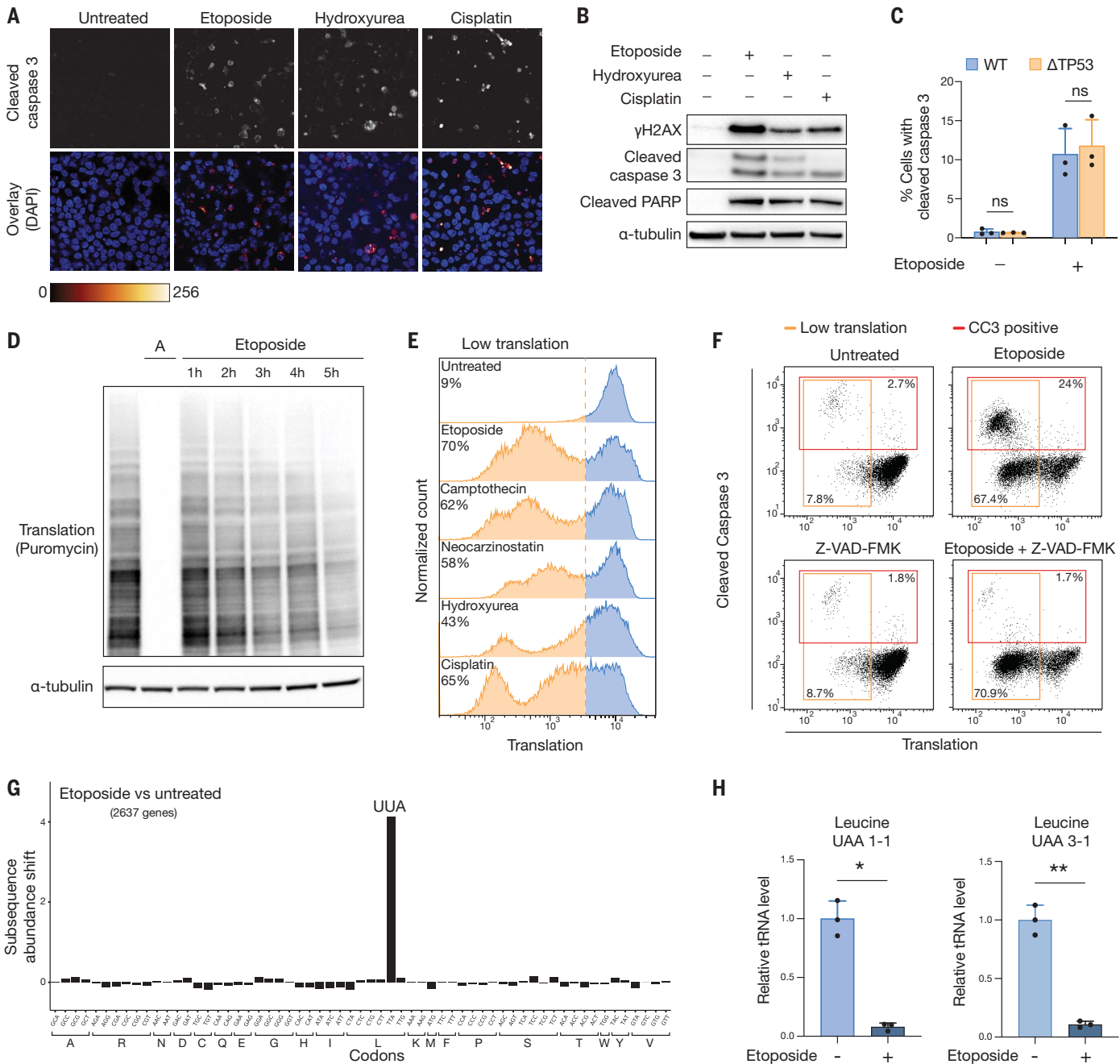†These authors contributed equally to this work.

DNA damage inhibits translation

To examine p53-independent apoptosis induced by DNA damage, we first established that human haploid HAP1 cells underwent apoptosis in response to exposure to etoposide, cisplatin, or hydroxyurea, which induce DNA damage by different mechanisms. HAP1 cells are derived from a chronic myeloid leukemia cell line and contain the *BCR-ABL* oncogene, which is not required for cell fitness (fig. S1A) (*8*, *9*). To detect the induction of apoptosis and distinguish it from other forms of cell death, we measured features of apoptotic cell death (fig. S2, A to D) and activation of the executioner caspase cleaved caspase-3 (Fig. 1A). Indeed, all treatments caused DNA damage, as indicated by the phosphorylation of Ser[139] on H2A histone family member X (γH2AX), and induced apoptosis (Fig. 1B). Because HAP1 cells contain a mutation in *TP53* affecting its DNA-binding domain (*10*), and some stimuli activate p53-independent apoptosis (*11*–*14*), this response was likely independent of p53. To address this, CRISPR-Cas9 was used to inactivate *TP53* in HAP1 cells or A549 cells that contain wild-type *TP53* (fig. S3A). In polyclonal cell populations, the wild-type cells and the cells that lacked p53 expression due to CRISPR editing underwent apoptosis in response to etoposide (Fig. 1C and fig. S3, B and C). Thus, DNA damage–induced apoptosis occurred independently of p53 in multiple cell types.

We further characterized the cellular response to etoposide in HAP1 cells and noticed a global decrease in protein synthesis by measuring the incorporation of puromycin in nascent peptides (Fig. 1D). Although an effect of radiation, and some chemotherapeutics, on global translation has been reported, the cause and function remain unclear (*15*–*19*). When measured at the single-cell level, it was evident that a subset of cells displayed low amounts of transla-tion upon exposure to different DNA-damaging agents (Fig. 1E and fig. S4, A and B). We measured translation and the activation of caspase-3 simultaneously in single HAP1 cells and found that DNA damage–induced caspase activation was only detected in the "low translation" cell population (Fig. 1F and fig. S3D), which was unaffected by BCR-ABL inhibition (fig. S3E). Inhibition of translation was unaffected by the cotreatment of cells with the pan-caspase inhibitor Z-VAD-FMK (Fig. 1F), which inhibited caspase activation. Thus, DNA damage selectively activates apoptotic caspases in cells with inhibited translation, and caspase activation itself was not required for the inhibition of translation.

DNA damage causes ribosome stalling

To investigate translation inhibition after DNA damage further, we used ribosome profiling to analyze the ribosome-protected fragments (RPFs) of mRNA. Metagene examination of the RPF distribution revealed an etoposide-induced accumulation of ribosomes at the translation start site (fig. S5A). To examine patterns of ribosome occupancy at the codon level, we used differential ribosome codon reading (diricore) (*20*, *21*). Subsequence (codon occupancy) and 5′-RPF density analyses demonstrated an increase in ribosome occupancy at RPF position 15 (corresponding to the ribosomal A site) on rare leucine UUA codons upon etoposide treatment, which was not observed on other codons and in particular other leucine codons (Fig. 1G and fig. S5B). These observations indicate that translation initiation was suppressed and ribosomes were stalled on the rare leucine codon UUA in response to DNA damage. Because the leucine UUA codon is not present in every protein, we investigated whether the accumulation of ribosomes at the translation start site occurred in the ~30% of all proteins devoid of leucine UUA codons. This showed that the reduction in translation initiation occurred on transcripts irrespective of the presence of UUA codons (fig. S5, C and D). To explore whether the stalling was caused by a shortage of the UUA-corresponding tRNA (tRNA[UUA]), we measured the abundance of the tRNA[UUA] by quantitative polymerase chain reaction (qPCR). Treatment of cells with etoposide resulted in a decreased abundance of tRNA[UUA] in the nucleus and cytosol (Fig. 1H and fig. S6, A and B). Our results show that DNA damage leads to a global decrease in translation, as well as specific ribosomal stalling on rare leucine-encoding UUA codons associated with a decreased abundance of the corresponding tRNA.

Translation inhibition and ribosome stalling require SLFN11

To study how DNA damage inhibits translation, we designed genetic screens in mutagenized

Fig. 1. DNA damage induces a global decrease in translation and ribosome stalling on the rare leucine codon UUA. (**A** and **B**) HAP1 cells treated with hydroxyurea (HU, 2mM) for 16 hours, cisplatin (2.5 μM) for 16 hours, and etoposide (5 μM) for 4 hours were subjected to immunostaining (A) and immunoblot analysis (B). (**C**) Quantification of three independent flow cytometry experiments comparing the proportion of HAP1 cells containing cleaved caspase-3 between wild-type and *TP53*-null cells after treatment with etoposide (5 μM) for 4 hours. HAP1 cells were infected with a CRISPR/Cas9 virus targeting *TP53* to obtain a mixed-cell population with wild-type and *TP53*-deficient cells and stained for p53 as well as cleaved caspase-3. *P* values were calculated using a two-tailed *t* test. ns, not significant. Data are shown as mean ± SD. (**D**) HAP1 cells were treated with either etoposide (5 μM) for 1 to 5 hours or anisomycin (5 μg/ml) (A) for 1 hour, followed by puromycin incorporation (2 μg/ml) for 10 min and immunoblot analysis. (**E**) Global translation was measured by flow cytometry in HAP1 cells treated with etoposide (5 μM) for 4 hours, neocarzinostatin (NCS, 500 ng/ml) for 4 hours, camptothecin (CPT, 1 μM) for 4 hours, HU (2 mM) for 16 hours, and cisplatin (2.5 μM) for 16 hours, followed by puromycin incorporation (2 μg/ml) for 10 min. Puromycin staining intensity was normalized between measurements (fig. S4). (**F**) Global translation (*x* axis) and caspase-3 cleavage (*y* axis) were measured by flow cytometry in HAP1 cells treated with etoposide (5 μM) for 4 hours and/or the caspase inhibitor Z-VAD-FMK (100 μM), followed by puromycin incorporation (2 μg/ml) for 10 min. (**G**) Diricore analysis bar plot depicting differential codon occupation (at position −15 of the RPFs) in etoposide-treated (5 μM for 3 hours) versus untreated HAP1 cells. (**H**) Real-time qPCR analysis of the UUA-corresponding tRNAs-UAA 1-1 and 3-1 normalized to U6 snRNA in HAP1 cells treated with etoposide (10 μM) in the presence of Z-VAD-FMK (100 μM) for 8 hours.

HAP1 cells. We used puromycin incorporation in nascent proteins of cells exposed to etoposide as a phenotypic readout that could be captured by fluorescence-activated cell sorting (FACS). Cell populations with relatively "high" and "low" signals of puromycin incorporation were isolated, and gene-trap insertions were mapped by deep sequencing (*22*). To identify genes required for the inhibition of translation, we looked for those that were enriched for disruptive mutations in the "high-translation" versus the "low-translation" cell population (Fig. 2A). We performed two screens in parallel in which the cells were either untreated or treated with etoposide (Fig. 2B; fig. S7, A and B; and tables S1 and S2). *Schlafen family member 11 (SLFN11)* and *general control nonderepressible 2 (GCN2)* were two of the most enriched genes present only in the etoposide-treated screen. GCN2 is a kinase phosphorylating eukaryotic translation initiation factor 2A (eIF2α) that
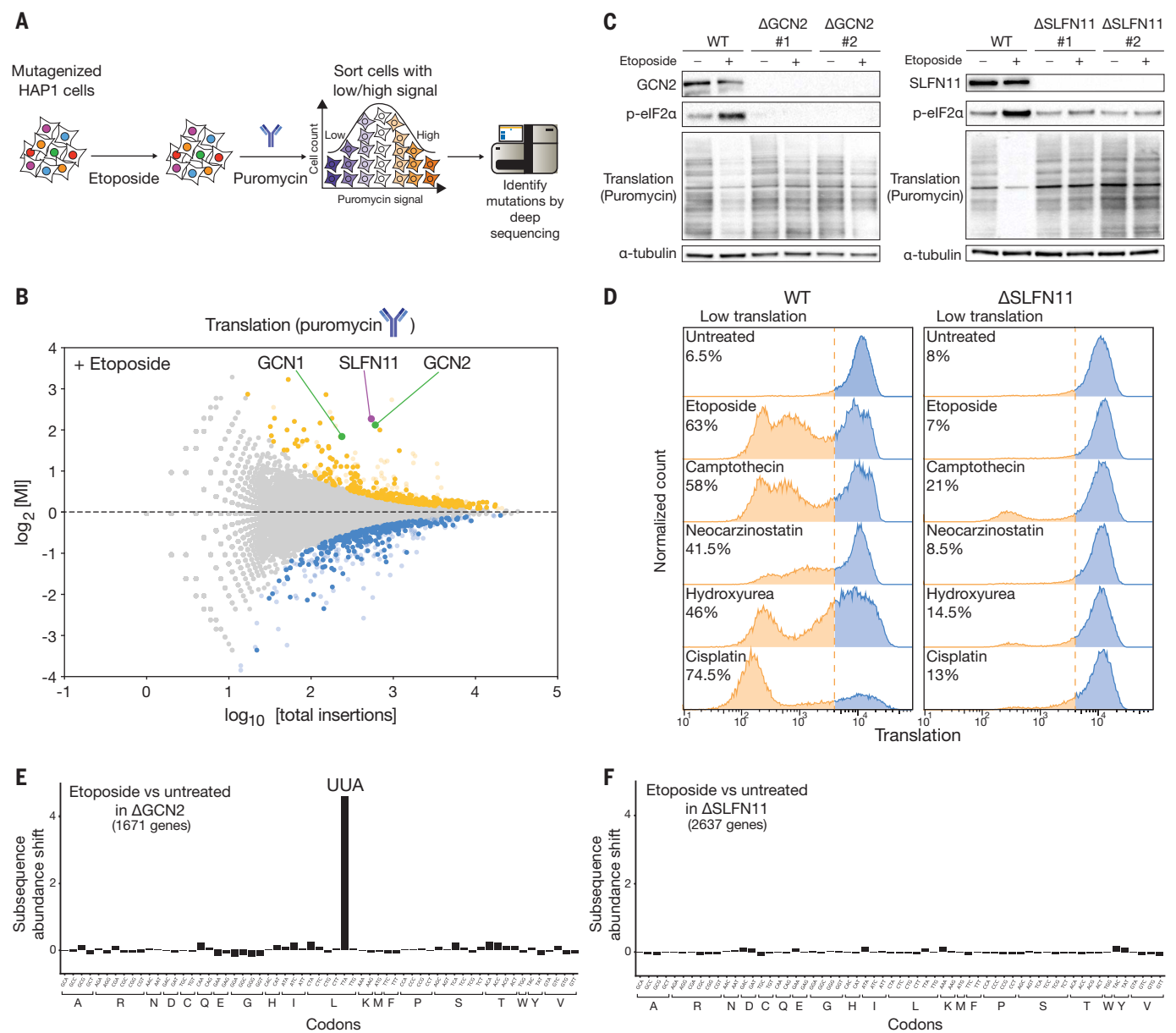
Fig. 2. SLFN11 is critical for ribosomal UUA stalling and GCN2 mediates global inhibition of translation. (**A**) Schematic representation of a haploid genetic screen to identify genes involved in DNA damage–induced inhibition of translation. (**B**) Genes that influenced translation after treatment with etoposide (5 µM) for 3 hours measured by puromycin incorporation (2 µg/ml) for 10 min and flow cytometry are presented as a fishtail plot. Genes are plotted according to their mutational index (MI) (y axis) and the total number of gene-trap insertions (x axis), with positive and negative regulators shown in blue and orange, respectively. Genes that were significant outliers in the untreated screen (fig. S7A) are displayed at 50% opacity. (**C**) Global translation

and eIF2α phosphorylation were visualized by immunoblot analysis in parental HAP1 cells and two independent *GCN2*-deficient (left) and *SLFN11*-deficient (right) clones treated with etoposide (5 µM) for 3 hours, followed by puromycin incorporation (2 µg/ml) for 10 min. (**D**) Global translation was measured by flow cytometry in parental HAP1 and *SLFN11*-deficient cells treated with etoposide (5 µM) for 4 hours, NCS (500 ng/ml) for 4 hours, CPT (1 µM) for 4 hours, HU (2 mM) for 16 hours, or cisplatin (2.5 µM) for 16 hours, followed by puromycin incorporation (2 µg/ml) for 10 min. (**E** and **F**) Diricore analysis bar plots depicting differential codon occupation (at position −15 of the RPFs) in etoposide-treated versus untreated *GCN2*-deficient (left) and *SLFN11*-deficient (right) HAP1 cells.

responds to amino acid starvation or ribosomal perturbations, but not to DNA damage, as part of the integrated stress response (ISR) with general control nonderepressible 1 (GCN1) as a coactivator (16, 23–26), which was also detected in the screen (Fig. 2B). *SLFN11* encodes a tRNAse that has been implicated in viral restriction and DNA damage sensitivity (27–30) and is frequently inactivated in tumor cells by promoter methylation (31–36). The effects of SLFN11 on sensitivity to DNA damage have been explained by its ability to stall stressed replication forks or to reduce the abundance of ataxia telangiectasia and Rad3-related (ATR) kinase (28, 29). SLFN11 was the most highly expressed member of the SLFN family proteins in HAP1 cells (fig. S7C) (22) and the only *SLFN* gene that was detected in the genetic screen (fig. S7D). In HAP1 cells, SLFN11 deficiency did not affect the abundance or activity

of ATR or ataxia telangiectasia mutated protein (ATM) kinase in response to DNA damage (fig. S8, A to C). We used HAP1 cells deficient for either SLFN11 or GCN2 to confirm that these factors had a role in the inhibition of translation in response to etoposide (Fig. 2C). *SLFN11*-null cells were also exposed to several DNA-damaging agents, and deficiency of SLFN11 impaired the inhibition of translation in all cases (Fig. 2D). DNA damage also induced eIF2α phosphorylation, which was absent in *GCN2*- and *SLFN11*-deficient cells, indicating that SLFN11 functions upstream of GCN2 (Fig. 2C).

Ribosomal footprinting of *SLFN11*- and *GCN2*-null cells showed that whereas GCN2 deficiency did not affect etoposide-induced UUA stalling, this response and tRNA^{UUA} downregulation was absent in cells lacking SLFN11 (Fig. 2, E and F, and fig. S9A). Because SLFN11 cleaves certain class II tRNAs, including

tRNA^{UUA} (28, 37), and SLFN11-induced tRNA cleavage was observed in cells exposed to DNA damage (28), we tested whether its tRNA endoribonuclease activity was required. Conditional expression of wild-type, but not an E209A SLFN11 mutant that is unable to cleave tRNAs (37), reduced the abundance of tRNA^{UUA} and elicited a global decrease in translation in HAP1 cells deficient for endogenous SLFN11 (fig. S9, B to D). Expression of wild-type but not E209A mutant SLFN11 in 293T cells, which normally do not express SLFN11 (fig. S9E) (27), allowed the DNA damage–induced inhibition of translation (fig. S9, E and F). Whereas SLFN11 cleaves multiple class II tRNAs (28), stalling occurred on the rarely used leucine codon UUA. Compared with other leucine codons, UUA appears most sensitive to perturbation because this is also the codon at which translation stalls upon leucine deprivation (38). That
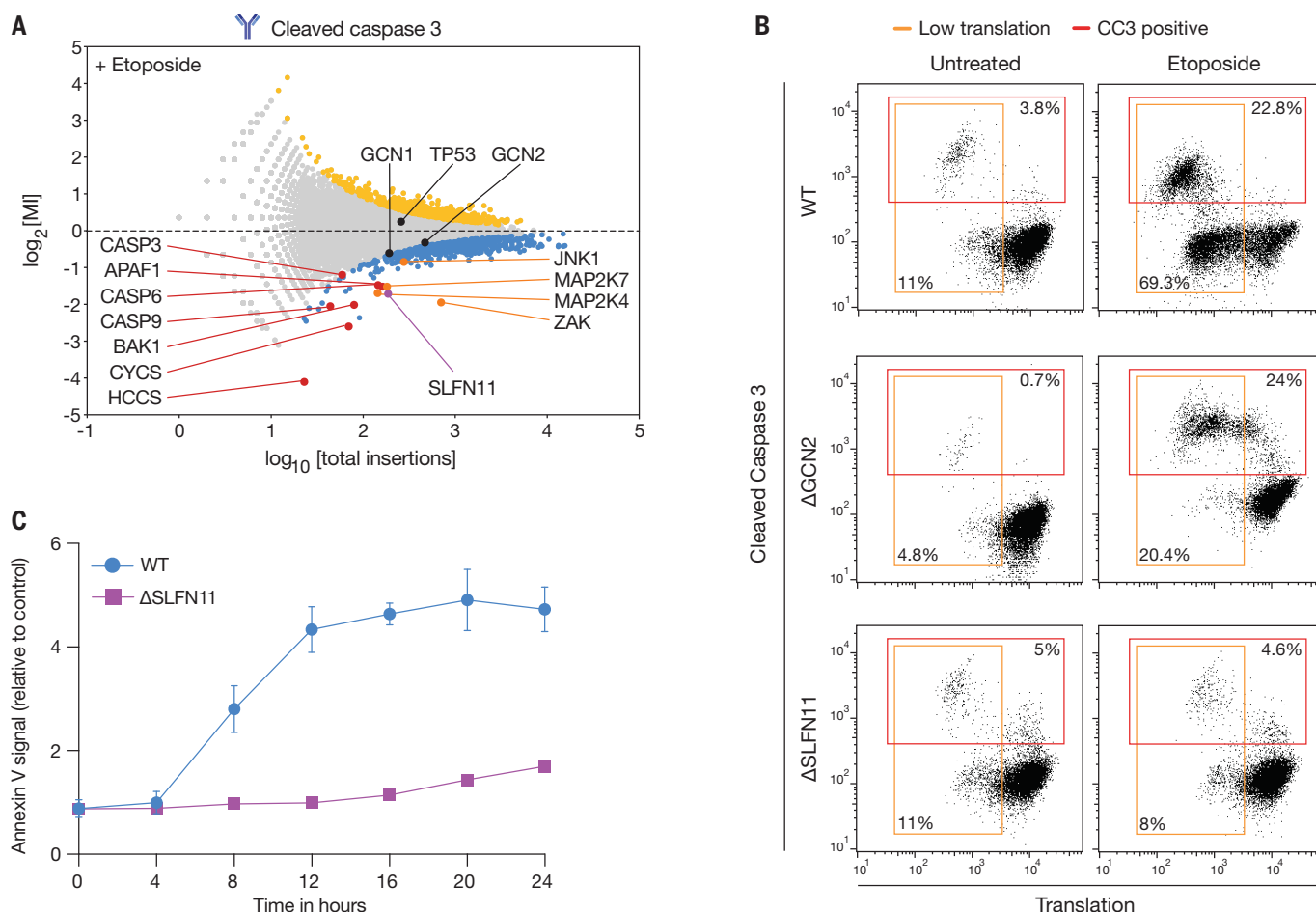
Fig. 3. DNA damage activates p53-independent apoptosis through *SLFN11*.
(**A**) Haploid genetic screen for the induction of apoptosis induction after treatment with etoposide (5 µM) for 4 hours as measured by cleavage of caspase-3. Genes are plotted according to their MI (*y* axis) and the total number of gene-trap insertions (*x* axis), with positive and negative regulators shown in blue and orange, respectively. (**B**) Global translation (*x* axis) and caspase-3 cleavage (*y* axis) were measured by flow cytometry in parental HAP1, *GCN2*-deficient, and *SLFN11*-deficient cells treated with etoposide (5 µM) for 4 hours, followed by puromycin incorporation (2 µg/ml) for 10 min. (**C**) Live-cell imaging was performed by the Incucyte ZOOM to measure the induction of apoptosis through Annexin V staining. Wild-type and *SLFN11*-deficient cells were exposed to etoposide, and images were taken every 4 hours for 24 hours.
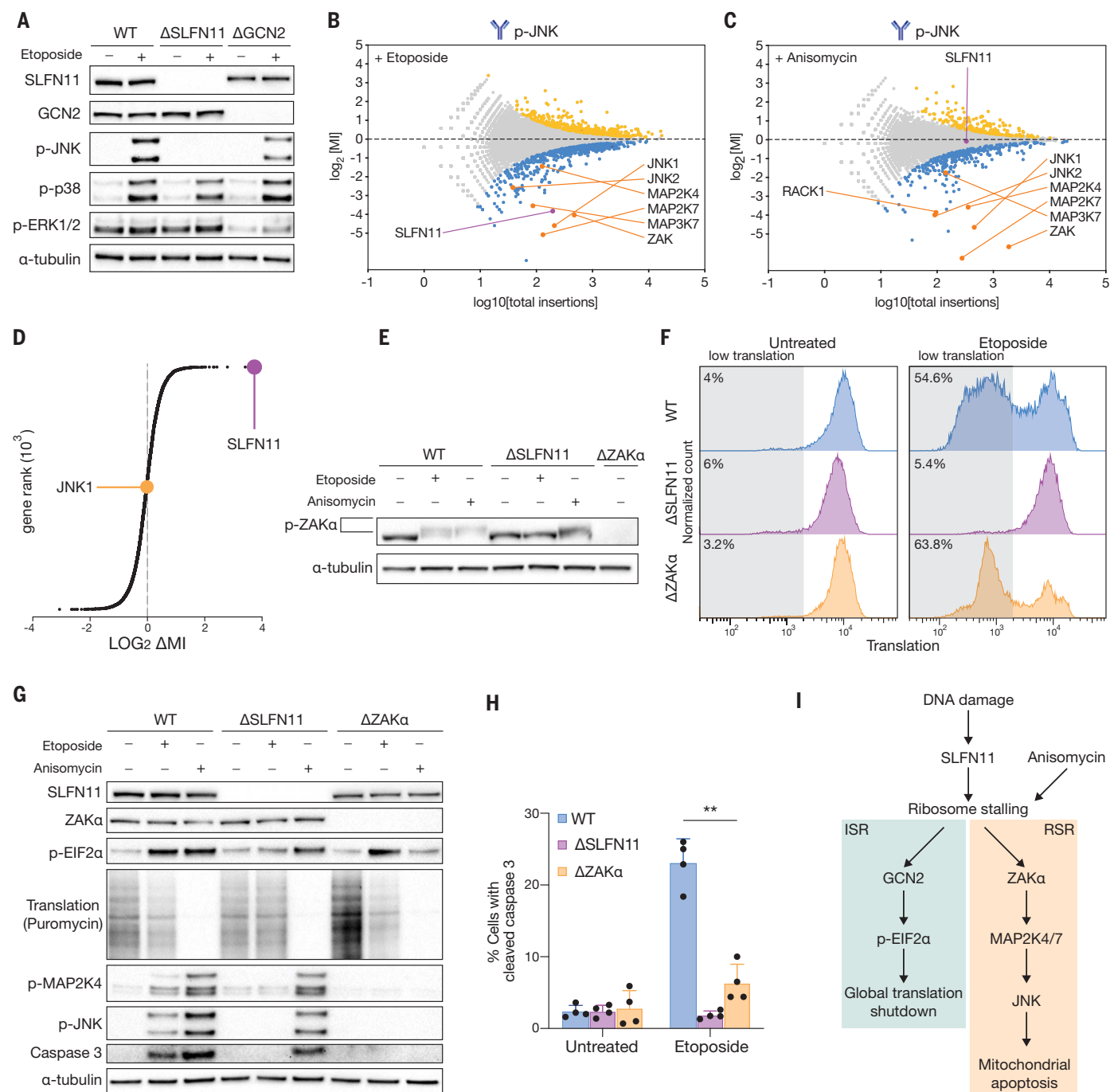
Fig. 4. SLFN11-induced ribotoxic stress activates ZAKα and causes MAPK-dependent apoptosis. (**A**) Parental HAP1, *GCN2*-deficient, and *SLFN11*-deficient cells were treated with etoposide (5 μM) for 3 hours and subjected to immunoblot analysis. (**B** and **C**) Haploid genetic screens for JNK phosphorylation after 3 hours of etoposide (5 μM) treatment (B) or 1 hour of anisomycin (5 μg/ml) treatment (C). Genes are plotted according to their MI (*y* axis) and the total number of gene-trap insertions (*x* axis), with positive and negative regulators shown in blue and orange, respectively. (**D**) Difference in MI (log₂) between the p-JNK screen treated with etoposide versus anisomycin for every gene with at least 30 insertions in both screens. (**E**) Phosphorylation of ZAKα determined by Phos-tag gel electrophoresis followed by immunoblot analysis. Cells were treated with etoposide (10 μM) in the presence of Z-VAD-FMK (100 μM) for 8 hours before cell lysis. (**F**) Translation was measured by flow cytometry in parental HAP1, *SLFN11*-null, and *ZAKα*-null cells treated with etoposide (5 μM) for 4 hours. (**G**) Parental HAP1, *SLFN11*-null, and *ZAKα*-null cells were treated with etoposide (5 μM) for 4 hours or anisomycin (5 μg/ml) for 1.5 hours, followed by puromycin incorporation (2 μg/ml) for 10 min and subjected to immunoblot analysis. (**H**) Quantification of four independent flow cytometry experiments measuring the proportion of cells containing cleaved caspase-3 in parental HAP1, *SLFN11*-null, and *ZAKα*-null cells treated with etoposide (5 μM) for 4 hours. *P* values were calculated using a two-tailed *t* test, **$P < 0.005$. Data are shown as mean ± SD. (**I**) Schematic depiction that illustrates how ribosome stalling by SLFN11 (upon DNA damage) or anisomycin leads to activation of the ISR and RSR by GCN2 and ZAKα, respectively.
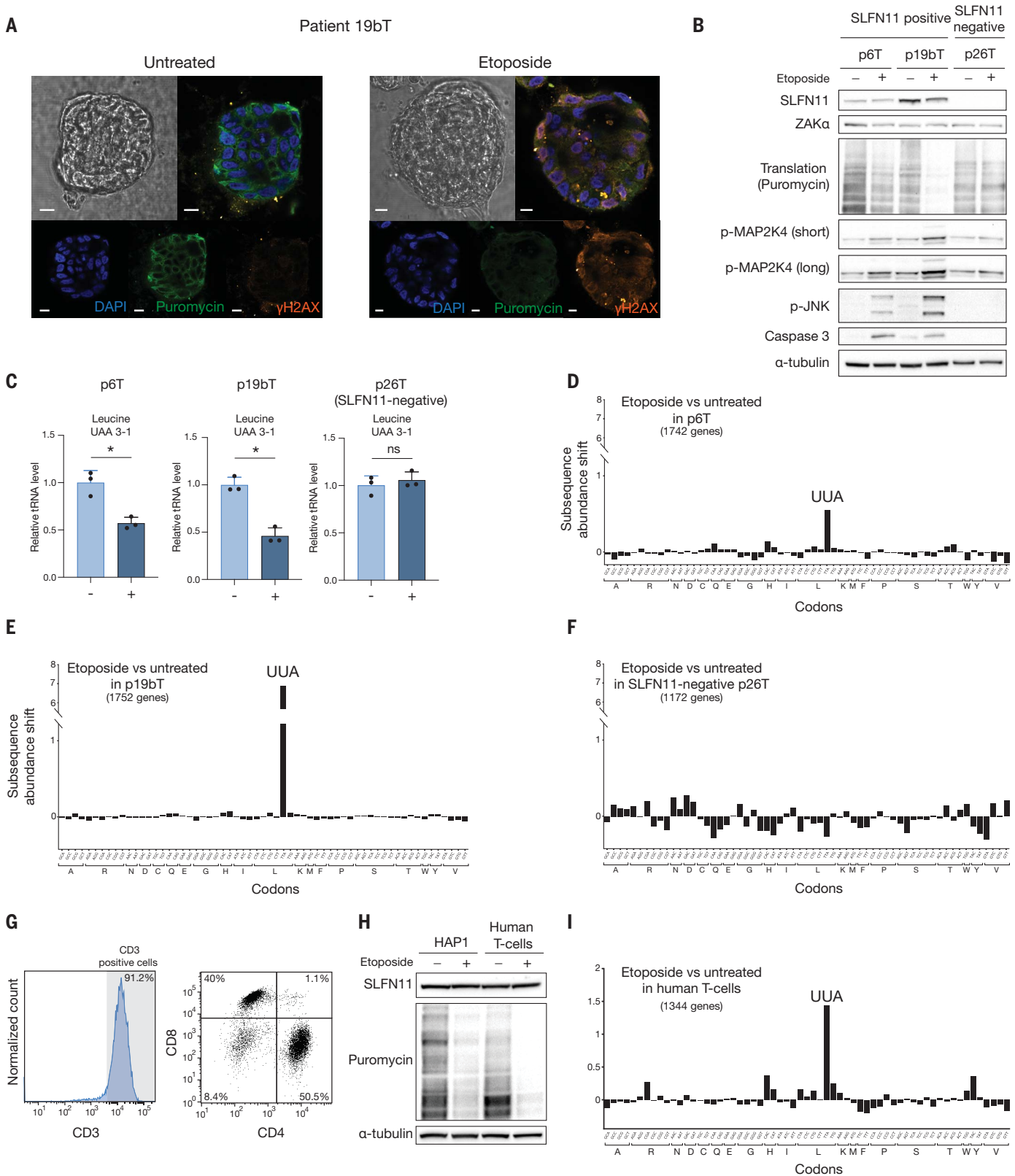
Fig. 5. DNA damage induces tRNA^UUA degradation, inhibition of translation, and ribosomal UUA stalling in patient-derived tumor organoids and primary human T cells. (A) Bright-field images taken of colon cancer organoids from p19bT either untreated or treated with etoposide (33 μM) for 18 hours followed by puromycin (10 μg/ml) for 10 min. The colon cancer organoids were subjected to immunostaining for γH2AX, puromycin, and 4′,6-diamidino-2-phenylindole (DAPI). Scale bar, 10 μM. **(B)** Colon cancer organoids p6T, p19bT, and p26T were treated with etoposide (33 μM) for 18 hours (p6T and p19bT) or 24 hours (p26T), exposed to puromycin (10 μg/ml) for 10 min, and subjected to immunoblot analysis. **(C)** Real-time qPCR analysis of tRNA-UAA 3-1 normalized to U6 snRNA in the

organoids p6T, p19bT, and p26T treated with etoposide (33 μM) for 18 hours (p6T and p19bT) or 24 hours (p26T). (**D** to **F**) Diricore analysis bar plot depicting differential codon occupation (at position –15 of the RPFs) in etoposide-treated (33 μM) versus untreated tumor organoids p6T (18-hour treatment), p19bT (18-hour treatment), and p26T (24-hour treatment). (**G**) Number of healthy primary human T cells positive for CD3 and subsequently CD4 (*x* axis) and CD8 (*y* axis) as measured by flow cytometry. (**H**) Human T cells and HAP1 cells were treated with etoposide (10 μM) for 12 hours (T cells) or etoposide (5 μM) for 4 hours (HAP1), followed by puromycin incorporation (2μg/ml) for 10 min, and subsequently subjected to immunoblot analysis. (**I**) Diricore analysis bar plot depicting differential codon occupation (at position –15 of the RPFs) in etoposide–treated (10 μM for 12 hours) versus untreated human T cells.

UUA is an important codon for Schlafen proteins to induce ribosome stalling is further supported by the notion that SLFN12 also selectively depletes the corresponding tRNA^UUA (*39*). Thus, in response to DNA damage, SLFN11 induces ribosomal UUA stalling and triggers a global inhibition of translation that requires GCN2.

SLFN11 mediates p53-independent apoptosis

To explore how the global translation inhibition and ribosomal UUA stalling might be connected, we designed an unbiased genetic screen to identify genes required for the induction of apoptosis by etoposide. We exposed gene-trapped HAP1 cells to etoposide and used cleaved caspase-3 staining as a phenotypic readout (Fig. 3A and table S3). This screen highlighted genes encompassing the mitochondrial death pathway [*BAK1* (*BCL2 antagonist/killer 1*), *cytochrome c*, *holocytochrome c synthase*, *APAF1* (*apoptotic peptidase activating factor 1*), *and caspase-9*] and the MAP-kinase signaling pathway [*JNK1* (*c-Jun N-terminal kinase 1*), *MAP2K7* (*mitogen-activated protein kinase kinase 7*), *MAP2K4* (*mitogen-activated protein kinase kinase 4*), and *ZAK* (*mitogen-activated protein kinase kinase 20*)], as well as *SLFN11* as factors needed for caspase-3 activation. *TP53* was not detected, and neither *GCN1* nor *GCN2* scored strongly. When global translation and caspase-3 activation were measured in single cells, it was evident that GCN2 was not required for activation of caspase-3. In contrast to wild-type cells, *GCN2*-null cells that did not show a prominent inhibition of translation still underwent apoptosis (Fig. 3B). Although GCN2 loss attenuated the global translation inhibition, a decrease in translation was still observed in these cells, which was most evident in cells treated with caspase inhibitors (fig. S10A). Loss of SLFN11 abolished both the global translation inhibition and the activation of apoptosis by etoposide but not by interferon-γ, a nongenotoxic agent that also causes translation inhibition and caspase-3 cleavage (Fig. 3B and fig. S11, A to C). Furthermore, SLFN11 was critical for the efficient activation of cell death in response to various DNA-damaging agents (Fig. 3C and fig. S10, B to F). Ultraviolet (UV) radiation leads to ribosome stalling and the activation of apoptosis in HeLa cells that do not express SLFN11, which occurs through UV-induced RNA damage (*40*). In agreement with this, *SLFN11*-deficient HAP1 cells showed inhibited translation and apoptosis in response to UV, albeit to a re-

duced extent compared with *SLFN11*-proficient cells (fig. S12A). Inhibition of neither ATR nor ATM affected etoposide-induced apoptosis after 4 hours (fig. S13, A and B); however, as observed previously, *SLFN11*-deficient cells were sensitized to DNA damage upon ATR inhibition after 24 hours, which was accompanied by SLFN11- and p53-independent apoptosis (fig. S13, C and D) (*28, 41, 42*). Thus, SLFN11-induced UUA stalling, but not GCN2-dependent global inhibition of translation, is critically required for the efficient induction of apoptosis in response to DNA damage.

To further investigate the interplay between the various molecular functions of SLFN11, we endogenously mutated codon E209A in *SLFN11* in HAP1 cells (fig. S14, A and B). When we examined global inhibition of translation, apoptosis, and cell viability, the E209A SLFN11 mutant HAP1 cells phenocopied SLFN11 deficiency (fig. S14, C and D). To ensure that this was not a clonal effect in the edited cell line, this was verified using a polyclonal pool of *SLFN11*-deficient HAP1 cells engineered to express wild-type or E209A SLFN11 in an inducible manner, and only wild-type SLFN11 caused the phenotype (fig. S14, E and F). The observed role of SLFN11 in supressing DNA replication during DNA damage was fully retained in the E209A mutant lacking nuclease activity (fig. S15, A and B) (*43*), suggesting that tRNA cleavage, but not inhibition of replication, is critical for the induction of apoptosis in this context. We further examined how SLFN11 responds to DNA damage. Whereas mutation of the single-stranded DNA–binding domain of SLFN11 does not influence its enzymatic activity in vitro (*37*), it does attenuate SLFN11 recruitment to sites of DNA damage in cells (*44*) and abolishes the inhibition of translation and induction of apoptosis in response to DNA damage (fig. S16, A and B).

DNA damage–induced ribotoxic stress signaling activates apoptosis

In addition to mitochondrial cell death pathway components and SLFN11, several MAPK pathway members were also identified in the etoposide-induced caspase activation screen. To study their role, we first examined the activation of main MAP kinases extracellular signal-regulated kinase (ERK1/2), p38, and JNK by immunoblot analysis (Fig. 4A). The activation of JNK, a direct activator of the mitochondrial death pathway that scored in the caspase screen,

was fully dependent on SLFN11, whereas activation of ERK and p38 was not. To examine the signaling toward JNK in more detail, we designed two complementary genetic JNK activation screens in response to either etoposide or the translation inhibitor anisomycin (*40*), a compound that activates JNK through drug-induced ribosomal stalling (Fig. 4, B and C, and tables S4 and S5). Comparative analysis of these screens indicated that only DNA damage–induced JNK activation required *SLFN11* (Fig. 4D). Etoposide and anisomycin required the same MAPK pathway members to activate JNK phosphorylation. Analysis of the mutations that were enriched in the "low-JNK" or "low-caspase" populations indicated that specifically the α-isoform of ZAK (ZAKα) was required for this phenotype (fig. S17A). ZAKα senses ribotoxic stress resulting in activation and autophosphorylation (*40, 45*). A similar activation of ZAKα was observed in response to etoposide, which was dependent on SLFN11 (Fig. 4E). Consistent with earlier observations (*40*), eIF2α phosphorylation upon anisomycin-induced ribotoxic stress requires ZAKα. By contrast, in response to DNA damage, the eIF2α phosphorylation and global inhibition of translation required SLFN11 but not ZAKα (Fig. 4, F and G). In response to either treatment ZAKα was necessary for the downstream signaling toward its substrate, MAP2K4, leading to subsequent activation of JNK and caspase-3 (Fig. 4, G and H, and fig. S17B). Finally, SLFN11 deficiency abrogated the translation inhibition and downstream MAPK signaling in response to DNA damage; nonetheless, these cells remained proficient in inducing an apoptotic response to ribotoxic stress triggered by anisomycin (Fig. 4G). A similar role for SLFN11 was observed in inducing eIF2α phosphorylation and the MAPK signaling cascade upon exposure to cisplatin (fig. S17C). Collectively, these results demonstrate that SLFN11 triggers ribosome stalling in response to DNA damage, leading to the activation of GCN2 and ZAKα and thereby resulting in a global inhibition of translation and the induction of apoptosis, respectively (Fig. 4I).

Discussion

Whereas translational stalling can be caused by errors, toxins, or the shortage of amino acids, this work highlights DNA damage–induced ribosomal UUA stalling as a signaling event that can lead to apoptosis. The DNA damage

response described here was not only observed in cancer cell lines of diverse origin (PC3 and A549; figs. S18 and S19, A to I), but also occurred in different patient-derived organoids obtained from human colorectal cancer (Fig. 5, A to F; fig. S20, A to I; and table S6) (*46*). The detection of DNA damage–induced ribosomal UUA stalling in healthy primary human T cells raises the possibility that this may contribute to the unwanted side effects of genotoxic cancer therapies (Fig. 5, G to I, and figs. S20I and S21, A and B). The evolution of SLFN11 as a viral restriction factor, which requires its tRNAse activity to limit translation, may have endowed cells with a pathway that responds to widespread DNA damage (*27*). Whereas SLFN11 has a dual role in viral restriction and DNA damage, SLFN12, which does not react to DNA damage, induces similar ribosomal stalling in response to velcrin, an exogenous synthetic SLFN12 activator with antitumorigenic activity (*39, 47, 48*). The dual role for SLFN11 in viral immunity and cellular genotoxic stress signaling may resemble that of cGAS-STING, which induces an inflammatory state by sensing aberrant DNA derived from either pathogens or from endogenous nucleic acids exposed as a result of copious DNA damage (*49, 50*). *SLFN11* is frequently inactivated by promoter methylation in tumors and thus represents a pathway that, like the p53 pathway, is often defective in cultured cancer cell lines. This may explain why the response elucidated here was not described previously. The recognition of SLFN11 as the strongest biomarker for chemotherapy responsiveness (*31, 33–36*) suggests relevance for ribosomal stalling in the effectiveness of cancer therapy.

REFERENCES AND NOTES

1. D. P. Lane, *Nature* **358**, 15–16 (1992).
2. T. M. Gottlieb, M. Oren, *Semin. Cancer Biol.* **8**, 359–368 (1998).
3. J. S. Fridman, S. W. Lowe, *Oncogene* **22**, 9030–9040 (2003).
4. M. J. Garnett et al., *Nature* **483**, 570–575 (2012).
5. W. P. Roos, B. Kaina, *Trends Mol. Med.* **12**, 440–450 (2006).
6. A. V. Gudkov, E. A. Komarova, *Nat. Rev. Cancer* **3**, 117–129 (2003).
7. D. Hanahan, R. A. Weinberg, *Cell* **100**, 57–70 (2000).
8. S. Lekomtsev, S. Aligianni, A. Lapao, T. Bürckstümmer, *BMC Genomics* **17**, 739 (2016).
9. V. A. Blomen et al., *Science* **350**, 1092–1096 (2015).
10. T. Bürckstümmer et al., *Nat. Methods* **10**, 965–971 (2013).
11. L. M. McNamee, M. H. Brodsky, *Genetics* **182**, 423–435 (2009).
12. J. S. Lanni, S. W. Lowe, E. J. Licitra, J. O. Liu, T. Jacks, *Proc. Natl. Acad. Sci. U.S.A.* **94**, 9679–9683 (1997).
13. M. I. Aladjem et al., *Curr. Biol.* **8**, 145–155 (1998).
14. G. Afshar et al., *Cancer Res.* **66**, 4223–4232 (2006).
15. S. Braunstein, M. L. Badura, Q. Xi, S. C. Formenti, R. J. Schneider, *Mol. Cell. Biol.* **29**, 5645–5656 (2009).
16. K. A. Spriggs, M. Bushell, A. E. Willis, *Mol. Cell* **40**, 228–237 (2010).
17. I. R. Powley et al., *Genes Dev.* **23**, 1207–1220 (2009).
18. V. A. Halim et al., *Mol. Cell. Proteomics* **17**, 2297–2308 (2018).
19. C. Riepe et al., *FEBS J.* **289**, 3101–3114 (2022).
20. F. Loayza-Puch et al., *Nature* **530**, 490–494 (2016).
21. O. Bartok et al., *Nature* **590**, 332–337 (2021).
22. M. Brockmann et al., *Nature* **546**, 307–311 (2017).
23. S. A. Wek, S. Zhu, R. C. Wek, *Mol. Cell. Biol.* **15**, 4497–4506 (1995).
24. J. Dong, H. Qiu, M. Garcia-Barrio, J. Anderson, A. G. Hinnebusch, *Mol. Cell* **6**, 269–279 (2000).
25. H. Qiu, J. Dong, C. Hu, C. S. Francklyn, A. G. Hinnebusch, *EMBO J.* **20**, 1425–1438 (2001).
26. A. K. Padyana, H. Qiu, A. Roll-Mecak, A. G. Hinnebusch, S. K. Burley, *J. Biol. Chem.* **280**, 29289–29299 (2005).
27. M. Li et al., *Nature* **491**, 125–128 (2012).
28. M. Li et al., *Nat. Struct. Mol. Biol.* **25**, 1047–1058 (2018).
29. J. Murai et al., *Mol. Cell* **69**, 371–384.e6 (2018).
30. Y. Mu et al., *EMBO Rep.* **17**, 94–109 (2016).
31. G. Zoppoli et al., *Proc. Natl. Acad. Sci. U.S.A.* **109**, 15030–15035 (2012).
32. E. E. Gardner et al., *Cancer Cell* **31**, 286–299 (2017).
33. N. Aben, D. J. Vis, M. Michaut, L. F. A. Wessels, *Bioinformatics* **32**, i413–i420 (2016).
34. J. Barretina et al., *Nature* **483**, 603–607 (2012).
35. C. Winkler et al., *JCI Insight* **6**, e146098 (2021).
36. K. Shee, J. D. Wells, A. Jiang, T. W. Miller, *PLOS ONE* **14**, e0224267 (2019).
37. F. J. Metzner et al., *Nat. Commun.* **13**, 5464 (2022).
38. M. VanInsberghe, J. van den Berg, A. Andersson-Rolf, H. Clevers, A. van Oudenaarden, *Nature* **597**, 561–565 (2021).
39. S. Lee et al., *Nat. Chem. Biol.* **2022**, 1–10 (2022).
40. C. C. C. Wu, A. Peterson, B. Zinshteyn, S. Regot, R. Green, *Cell* **182**, 404–416.e14 (2020).
41. U. Jo et al., *Proc. Natl. Acad. Sci. U.S.A.* **118**, e2015654118 (2021).
42. J. Murai et al., *Oncotarget* **7**, 76534–76550 (2016).
43. F. Qi et al., *Genes Cells* **28**, 663–673 (2023).
44. E. Alvi et al., *Commun. Biol.* **6**, 1–12 (2023).
45. A. C. Vind et al., *Mol. Cell* **78**, 700–713.e7 (2020).
46. M. van de Wetering et al., *Cell* **161**, 933–945 (2015).
47. D. Li et al., *Mol. Cell* **75**, 1103–1116.e9 (2019).
48. C. W. Garvie et al., *Nat. Commun.* **12**, 4375 (2021).
49. L. Sun, J. Wu, F. Du, X. Chen, Z. J. Chen, *Science* **339**, 786–791 (2013).
50. J. Wu et al., *Science* **339**, 826–830 (2013).

SUPPLEMENTARY MATERIALS

science.org/doi/10.1126/science.adh7950
Materials and Methods
Figs. S1 to S21
Tables S1 to S6
References (*51–59*)
MDAR Reproducibility Checklist